

## DETERMINATION OF CHARACTERISTIC MICROSTRUCTURES IN SIMULATED AND REAL TIG AND LASER WELDMENTS OF OPTIM 960 QC STEEL

Sveto Cvetkovski<sup>1</sup>, Vencislav Grabulov<sup>2</sup>

<sup>1</sup>University Ss Cyril and Methodius, Faculty of Technology Metallurgy, Skopje, Republic of  
Macedonia

<sup>2</sup>Institute for testing of materials - IMS, Belgrade, Serbia

**Keywords:** *Optim 960 QC steel, HAZ, welding microstructure, Gleeble simulator, grain size.*

### Abstract

In this research work metallographic analysis of simulated and real microstructures in HAZ of Optim 960 QC was performed. Thin sheets (6 mm) were used for simulation and real TIG and laser welding. Special specimens were prepared for welding simulation. The peak temperatures corresponding to specific microstructures in the HAZ was obtained by performing welding using Gleeble 1500 welding simulator. The following parameters were used in the thermal simulation: heating rate: 500°C/s, peak temperature: 500, 600, 700, 800, 900, 1000, 1100, 1200, 1250, 1300 and 1350 °C/s, holding time: 1 s, cooling time,  $\square_{t_{8/5}}$ : 1,7 s (air cooling). Two autogenously TIG welding experiments using different welding heat input were carried out. Besides, CO<sub>2</sub> laser beam welding experiments were carried out too.

After performing welding simulation and real welding. metallographic preparation of specimen was done. Standard metallographic preparation of specimens was performed. Besides optical microscopy; scanning electron microscopy was used for microstructural analysis. Hardness measurements and determinations of grain sizes were performed on simulated metallographic specimens. Besides comparison of different micro constituents (real and simulated), the length of total HAZ in dependence of the heat input was analyzed too.

### 1. Introduction

Ultra-high strength steels with the minimum specific yield strengths of 960 MPa with the proprietary names Optim 960 QC, are made using hot strip rolling and direct quenching followed by leveling and cutting to plates with thicknesses in the range 2.5 – 8.0 mm. Due to thermo mechanical rolling combined with direct quenching and low carbon content, a good combination of strength, toughness and formability is achieved without tempering [1,2].

Optim QC steels are ultra-high-strength, formable and wear-resistant structural steels of high tensile strength. Their abrasion resistance is significantly better than that of common structural steels. The ultra-high strength good formability and weldability make possible the use of slender, light structures, which possess unique durability. In the development of these steels, the aim was to achieve the required yield strength levels in combination with good impact toughness, weldability, formability and suitability for hot dip galvanizing [3-5]. In addition, consideration was given to the increasing demand for suitability to laser cutting and welding [6,7].

Its main applications are: chassis and body work of commercial vehicles, booms of forest machinery, crane arms and other lifting equipment, load handling equipment, load support and fastening equipment, feeding and unloading hoppers containers, etc.

Suitable bainite/martensite hardenability is achieved by controlling the contents of alloying elements like Cr, Cu, Ni, Mo, Nb, V and B [5,6]. Therefore, the steel composition was based on as low carbon

content as possible in order to ensure good weldability, as defined by preheating requirements and heat affected zone toughness, good flangeability and suitability to laser processing. Silicon was limited to below 0.25% in order to ensure good hot dip galvanizing properties and to prevent any problems with red scale, which would impair surface quality. Manganese was maintained below 1.2%, which together with the low carbon content keeps centre-line segregation to a minimum and improves the flangeability of sheared edges. Similar advantages are gained by keeping phosphorus and sulphur contents low and by modifying the sulphide inclusions using calcium treatment [8-12]. The low carbon content imparts high impact toughness after direct quenching to bainite /martensite thereby eliminating the need for tempering. It also ensures good weldability without the need for preheating[13-15].

This steel is pretty easy to weld using all the normal methods when the instructions for high strength steels are adhered. When using high welding energy and/or low material thicknesses, a narrow zone of material softer than the parent metal may appear in the weld [16].

Characteristic martensitic/bainitic microstructure of Optim 960 QC steel is changing during welding as result of welding thermal cycles. So main idea in this research work was to determine and analyze characteristic micro constituents in HAZ and to make comparison between simulated microstructure and real microstructure formed in TIG and laser welding.

## 2. Material and experimental work

Designation of Optim 960 QC steel means the following: 960 is minimal yield strength of the steel in Mpa. The letter "Q" stands for quenching and the letter "C" for cold formability. Optim 960 QC steel sheets in 6 mm thickness from Rautaruukki Oyj was investigated in this work. Chemical composition, tensile properties and impact toughness at different temperatures are presented in Tables 1-3.

Table 1 Chemical composition of the investigated steel Optim 960 QC (wt-%):

C	Si	Mn	P	S	Al	Nb	V	
0.098	0.169	1.04	0.010	0.003	0.032	0.002	0.007	
Cu	Cr	Ni	N	Mo	Ti	B	CEV	P <sub>cm</sub>
0.031	1.07	0.057	0.0058	0.154	0.029	0.0020	0.52	0.23

Table 2 Tensile properties of Optim 960 QC steel

Specimen no.	Thickn. (mm)	Test direction	R <sub>p0.2</sub> (N/mm <sup>2</sup> )	R <sub>m</sub> (N/mm <sup>2</sup> )	A <sub>5</sub> (%)
63277-21	6	long.	1028	1120	12
63277-21	6	transv.	1038	1139	11

Table 3 Charpy-V impact properties of Optim 960 QC

Transverse:

Temp. (°C)	Charpy V specimen	Average (J)	Ductile fracture (%)
20	6x10 mm	76	100
0	6x10 mm	67	100
-20	6x10 mm	66	100
-40	6x10 mm	40	50
-60	6x10 mm	27	20
-80	6x10 mm	22	10

## 2.1 Welding experiments

Specimens simulating various HAZ zones and real weldments (TIG and Laser welding) were prepared from the experimental sheets. Two autogenous TIG welding experiments were carried out. The welding parameters employed are given in Table 4. Macro photos of bead on plates of TIG weldments are given in Figure 1, It is obvious from the figure 1 that much better penetration is obtain implementing higher welding parameters.

CO2 laser beam welding experiments were carried out at Lappeenranta University of Technology (LUT). The shielding gas was helium with a flow rate of 20 l/min. Applied parameters are given in Table 5. Macro photos of typical cross-sections of the weldments are shown in Figure 2.

Table 4 Welding parameters for autogenous TIG bead-on-plate welding

Parameters	Weld a	Weld b
Current (A)	150	190
Voltage (V)	12	14
Welding speed (mm/min)	250	250
Heat input Q (J/mm)	256	383

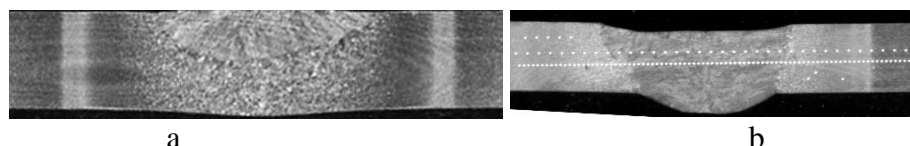


Figure 1 Macro photos of cross-sections of TIG bead-on-plate weldments, a) 256 kJ/mm, b) 383 kJ/mm

Table 5 Parameters for laser welding of Optim 960 QC

Weld no.	Sheet thick. mm	Laser power, W	Welding speed, m/min	Focal length, mm
9	6	5000	0.5	300
12	6	5000	2	300
29	6	5000	1	200
32	6	5000	3	200

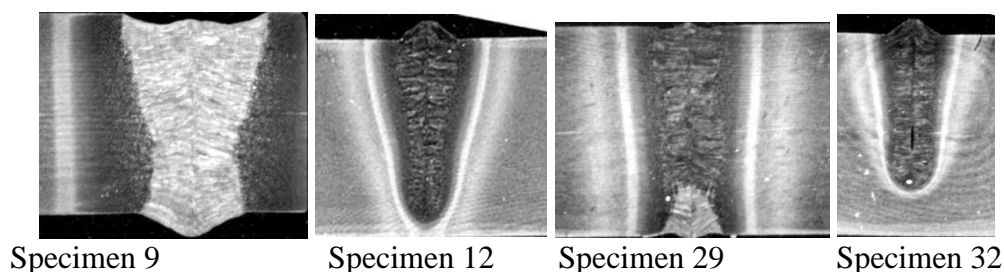


Figure 2 Macro photos of cross-sections of four laser welds

## 2.2 Welding simulation

Simulation of the influence of welding thermal cycles on microstructure of the HAZ was performed on a Gleeble 1500 simulator. The shape and dimensions of the specimens used for simulation experiments are shown in Figure 3.

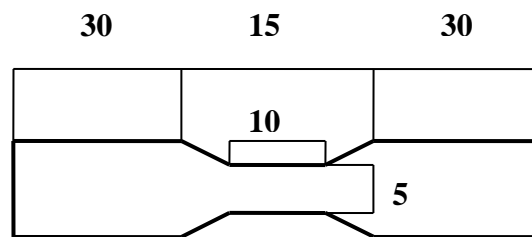


Figure 3 Shape and dimensions of the specimens for thermal simulation

The following parameters were used in the thermal simulation:

Heating rate: 500°C/s

Peak temperature: 900, 1000, 1100, 1200, 1250, 1300 and 1350 °C/s

Holding time: 1 s

Cooling time,  $t_{8/5}$ : 1,7 s (air cooling)

Thermal history in the simulation experiment until the different peak temperature in the range 900-1350°C and cooling time of 1.7 s (air cooling) are shown in Figure 4.

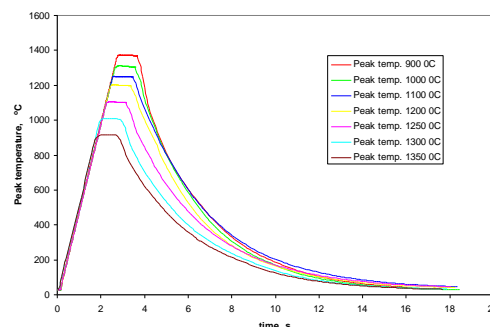


Figure 4 Simulation thermal curves: heating rate 500°C/s, holding time 1s, cooling time 1.7 s (air cooling)

After bead-on-plate welding (TIG and laser) and Gleeble thermal simulation, hardness measurements, grain size determination and metallographic investigations of microstructure were performed on simulated specimens and weldments. Hardness in the welded joints was measured along the line, at the distance of 0.5 mm below the surface and 0.2 mm between the measuring points. In all cases, the load of 2 kg was used. Nine measurements were made on every specimen and the hardness value is given as an average value.

Standard procedure for metallographic preparation was employed. Chemical etching was used for determination of primary austenite grain size. The composition of the etchant for simulated specimens is the following: 100 ml distilled water, 1.4 g picric acid, 1 ml a wetting agent (Agepon or Teepol), 075 -1 ml HCl. For etching of real welded joints was used Nital and for color etching was used LePerra etchant.

### 3. Result and Discussion

The influence of peak temperature on hardness values of simulated specimens is shown in Figure 5, and hardness values measured across the welded joints are plotted in Figure 6 (a and b).

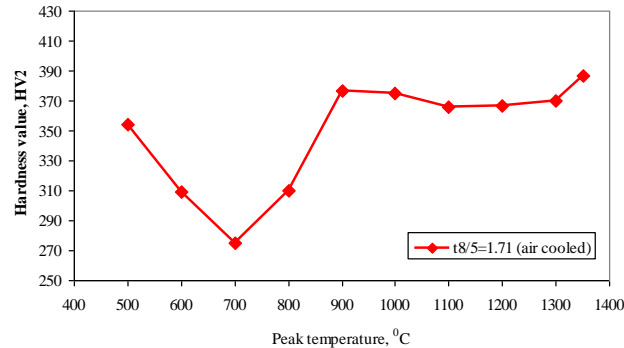


Figure 5 Hardness values in dependence on the simulation peak temperature

It can be seen in Figure 5 that the hardness drops with increasing temperature between 500-700°C, obviously due to softening by tempering of the martensitic structure of the steel. In the dual-phase area, sc. intercritical zone, roughly between 800°C and 900°C, the formation of austenite in heating and transforming back to hard martensite during fast cooling, and refined grain size, increase the hardness. Above 900°C, the hardness is quite constant, obviously due to complete austenite formation in heating and subsequent martensite formation upon cooling. Measured hardness at peak temperature of 900 °C is about 270 HV, and at peak temperature of 1350 °C about 390 HV.

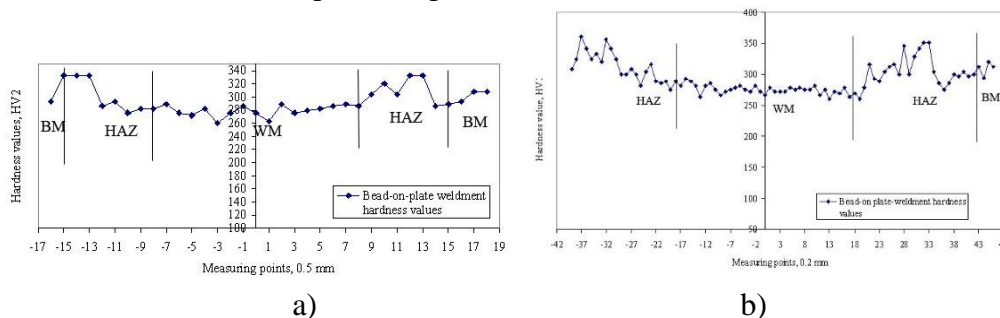


Figure 6 Hardness values across TIG welded joints, a) 256 kJ/mm b) 383 kJ/mm

It is characteristic for this type of steel that softened and hardened zones can appear in the HAZ. Softened zone is obvious (hardness below 300 HV in simulated specimens). Increase of hardness in the HAZ may be due to grain size refinement. But sharp hardened zone was not noticed, probably because of lower carbon content.

From the hardness values in Figure 6, it can be seen that the weldments does not contain a hardened zone too (hard martensite) near the fusion line.

Microstructure of direct quenched steel (base material) consists of lath martensite and bainite. The calculated hardness of martensite is  $372 \text{ HV} (H_m = 884 \cdot C(1 - 0,3 \cdot C^2) + 294)$ , while for the bainite it is 323 HV. Measured hardness values in the real TIG weldments are something lower than in simulated specimens.

Grain size determination was performed on simulated specimens using NIKON optical microscope with a device for quantitative measurements. Results are plotted in Figure 7. The refinement of grain size in the intercritical zone and low-austenite regime can be seen, and extensive grain coarsening at highest peak temperatures.

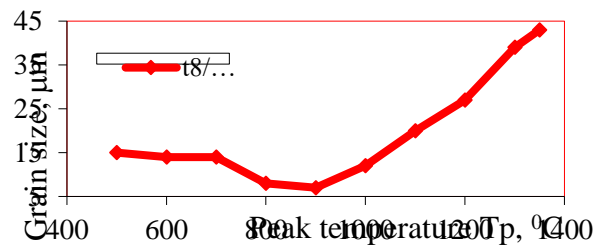


Figure 7 Grain size in dependence of peak temperature

It can be concluded from the diagram that the finest grain size is obtained for peak temperature of 900 °C. Microstructural investigations confirmed this conclusion.

As it can be seen from Figure 7 and Figure 8 (a), the largest grain size is obtained at the highest peak temperatures of 1300 and 1350°C (Figure 8 a). At lower peak temperatures between 1200 (Figure 8 b) and 1100°C, smaller, equiaxed grains, similarly as in the former case, are formed. Microstructure with mixed coarser and finer grains can be seen at the peak temperature of 1000 °C (Figure 8c), while very fine grains are detected at the peak temperature of 900 °C (Figure 8 d). It means that 900°C is just slightly above the A<sub>3</sub> temperature, where complete austenitic transformation has occurred.

Another approach was to calculate the phase transformation temperatures using experimental equations for the Ac<sub>1</sub> and Ac<sub>3</sub> temperatures.

$$Ac_1(^{\circ}C) = 739 - 22 * (\%C) + 2 * (\%Si) - 7 * (\%Mn) + 14 * (\%Cr) + 13 * (\%Mo) - 13 * (\%Ni) + (\%V)$$

$$Ac_3(^{\circ}C) = 902 - 255 * (\%C) + 19 * (\%Si) - 11 * (\%Mn) - 5 * (\%Cr) + 13 * (\%Mo) - 20 * (\%Ni) + 15 * (\%V)$$

The values from the calculation are: Ac<sub>1</sub>=746°C and Ac<sub>3</sub>=859°C. These values correspond very well with dilatometric experimentally determined values in another research.

Intercritical transformation is very clearly seen in Figure 8e revealing mixed grain size. Figure 8e and also SEM analysis (Figure 9b) indicates that transformation starts on grain boundaries, where first new austenite grains are located. Similar conclusions can be obtained from figure 9c where specimen heated to intercritical area is etched with LePerra reagent. Yellow color transformed austenite is located at grain boundaries. Figure 9a concern to specimens heated to peak temperature of 820 °C (t<sub>8/5</sub>=15s.). Similar microstructure like at peak temperature of 800 °C is obtained. At temperatures of 500 and 700 °C, only tempering of martensitic microstructure happens (Figure 8f). In accordance, Figure 5 shows that the hardness decreases in simulated specimens until the peak temperature of 700°C, as a result of the tempering process. SEM analysis (Figure 10a) showed that heating to peak temperature of 500°C contributes to precipitation of some particles, presumably carbides, mainly inside the grains. At the peak temperature of 700°C, coarser precipitates can be seen (Figure 10b) which precipitated at grain boundaries. Besides, there is precipitation inside the grains, too. There is no visible changes (detectable in optical microscope) in the microstructure in the specimen heated to the peak the temperature of 500 °C.

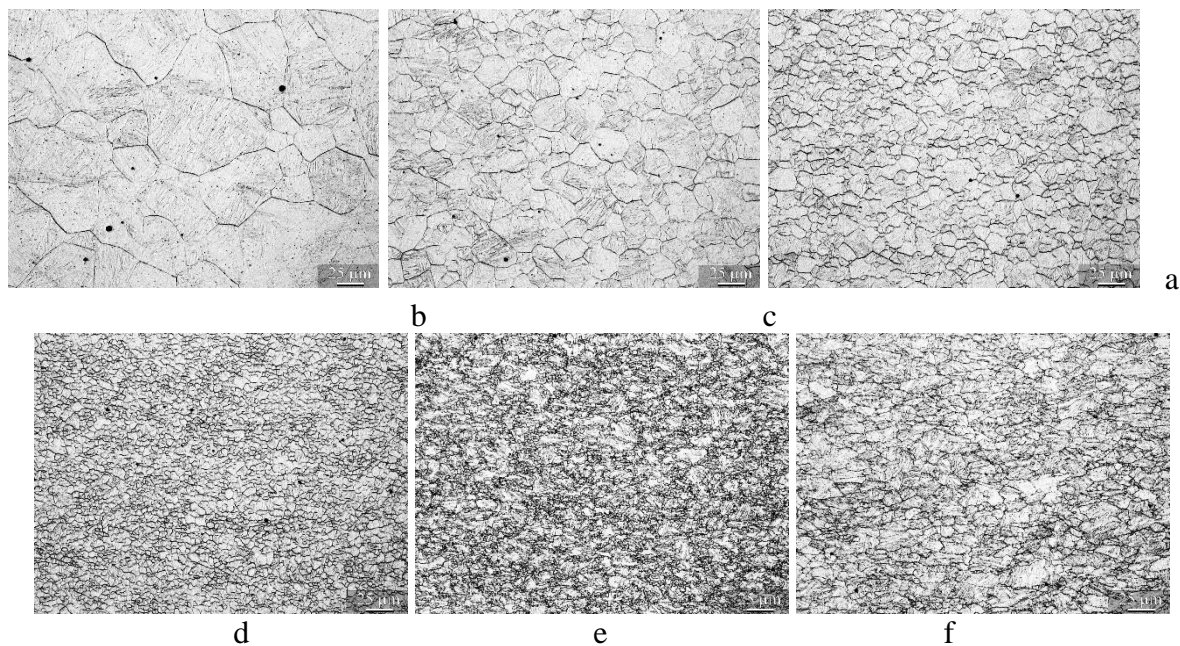


Figure 8 (a-j) Microstructures of specimens heated to the peak temperature of  
a) 1350 °C b) 1200 °C c) 1100 °C d) 1000 °C e) 800 °C f) 500

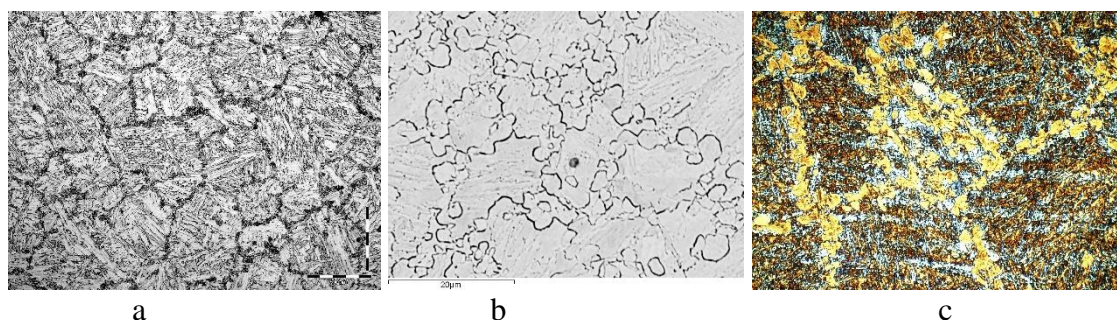


Figure 9. Microstructure of specimen heated to 800°C, SEM-BE image  
a. Simulated ICCGHAZ (820°C) with  $t_{8/5}=15s$ . b. SEM-BE image simulated specimen, c.  
Simulated ICCGHAZ with  $t_{8/5}=5 s$ . (LePera etching).

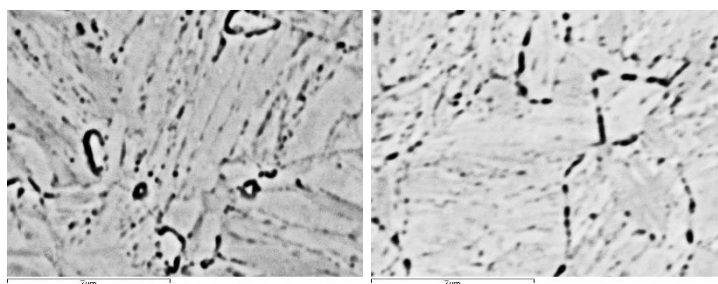


Figure 10 (a and b). a. Microstructure of specimen heated to 500°C, BE image b. Microstructure of specimen heated to 700°C, BE image

A general conclusion for the real weldments is that the HAZ microstructure of TIG and Laser weldments is very similar with the microstructure in simulated specimens.

All characteristic microstructures obtained by simulation at corresponding peak temperatures were found in the real HAZ. Such an example is given in Figure 11, where microstructures of simulated specimens at appropriate peak temperatures were found in the HAZ microstructure. The same etchant is used in both cases, but HAZ is slightly stronger etched.

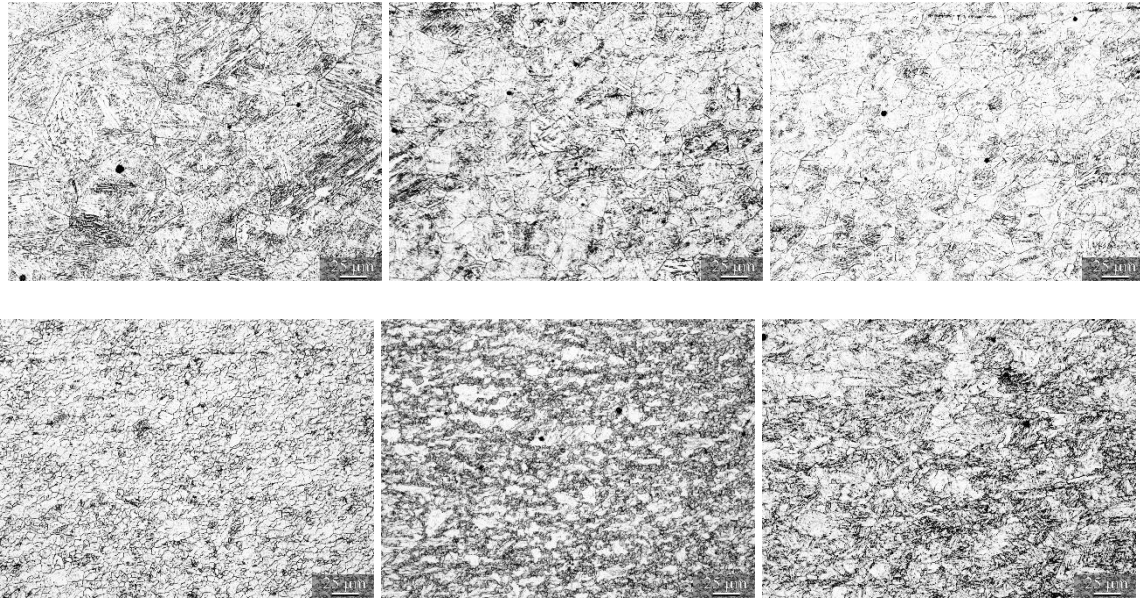


Figure 11 Microstructure of HAZ specimens and concerning HAZ of TIG weld

From the macro photos in Figures 1 and 2 it is obvious that the shape of the TIG and laser weldments, the depth of penetration and the width of HAZ, are strongly dependent on welding parameters employed. It can be seen from Figure 1 that full penetration is not achieved for the specimen 1a and 12 and 32 in Figure 2 for laser welding. In addition, it was observed that the grain size in laser welds is generally smaller than in simulated and TIG weldments.

Figure 12 presents completely microstructure of HAZ starting from the fusion line until the temperature of 800 °C. As can be seen total length of HAZ is determined. The length of the HAZ depends from the welding parameters. Melting temperature is calculated from the following equation:  $1800 - 90 * C$ .

Using the carbon content 0.098% (Table 1) of Optim 960 QC,  $T_m$  is 1518 °C.

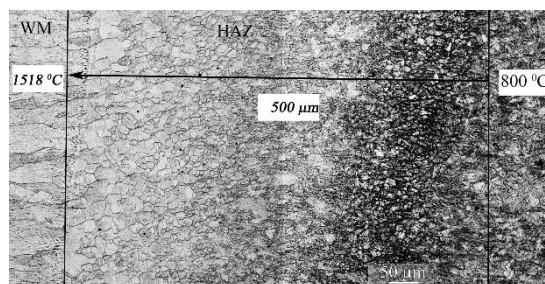


Figure 12 Measured distance 1518/800 °C laser bead-on-plate weldment, specimen 32

As can be seen from the figure 13a Epitaxial growth of columnar grains start from the partially melted grains and continue in weld metal. The end of HAZ is noticed in the figure 13b from ICHAZ to the base metal. It is the starting position of intercritical transformation.

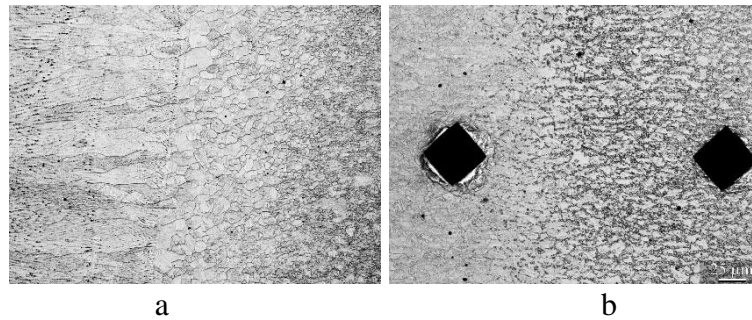


Figure 13 (a and b) a. Epitaxial growth of grains from the weld fusion line into the coarse grained HAZ

b. The edge of intercritical zone in the HAZ of Laser welded joint, specimen 32

#### 4. Conclusions

From the investigations performed in this research work the following conclusions were obtained: Microstructure of real weldments (TIG and Laser) corresponds very well with the microstructure of the specimens simulated at different peak temperatures.

The width of HAZ depends of the welding heat input.

Precipitation of carbides at 500 °C is inside the grains while at 700 °C carbides are mainly precipitated at gran grain boundaries.

The finest grains in the HAZ are formed at peak temperature 900 °C and the highest at the temperature of 1350 °C.

Softened zones appears at peak temperature of 700 °C

The hardness value at 700 °C is 270 HV while at 350 °C is 390HV.

Characteristic hardened zone didn't appear probably because of the lower carbon content

Intercritical transformation was noticed at peak temperatures of 800 °C. According calculation Ac1 temperature is 746 and Ac3 859 °C.

Austenitic transformations start at grain boundaries.

#### 5. References

- [1] Hot rolled steel Plates, Sheets and coils, Structural steels, Optim QC, [www.ruukki.com](http://www.ruukki.com)
- [2] HOT-ROLLED STEEL SHEETS, PLATES AND COILS. Welding general, [http://www.oxycoupage.com/FichiersPDF/Ruukki\\_Pdf/English/Ruukki-Hot-rolled-steels-Processing-of-material-Welding.pdf](http://www.oxycoupage.com/FichiersPDF/Ruukki_Pdf/English/Ruukki-Hot-rolled-steels-Processing-of-material-Welding.pdf)
- [3] Juha Nuutinen, Development trends in Finnish metal industry METNET Annual Seminar, Minsk, Belarus 21-22 October 2009
- [4] J. Kömi , “ Hot-rolled ultra-high-strength steels,” J. Mater. 1, 50–51 (2012),
- [5] M. Hemmilä, R. Laitinen, T. Liimatainen, D. Porter, MECHANICAL AND TECHNOLOGICAL PROPERTIES OF ULTRA HIGH STRENGTH OPTIM STEELS [http://www.oxycoupage.com/FichiersPDF/Ruukki\\_Pdf/English/Ruukki-Technical-article-Mechanical-and-technological-properties-of-ultra-high-strength-Optim-steels.pdf](http://www.oxycoupage.com/FichiersPDF/Ruukki_Pdf/English/Ruukki-Technical-article-Mechanical-and-technological-properties-of-ultra-high-strength-Optim-steels.pdf)
- [6]. RUUKKI, Optim QC structural steel, [http://www.oxycoupage.com/FichiersPDF/Ruukki\\_Pdf/English/Optim-QC-structural-steels.pdf](http://www.oxycoupage.com/FichiersPDF/Ruukki_Pdf/English/Optim-QC-structural-steels.pdf)
- [7] Jukka Siltanen, Laser and laser gas-metal-arc hybrid welding of 960 MPa direct-quenched structural steel in a butt joint configuration, Journal of Laser Applications 27, S29007 (2015); <http://dx.doi.org/10.2351/1.4906386>
- [8] J. Kömi , “ Direct-quenched structural steel,” Design Manual (2013).
- [9]. M. Hemmilä, R. Laitinen, T. Liimatainen, D. Porter, Mechanical and technological properties of ultra high strength Optim steels, Rautaruukki Oyj, Ruukki Production, Finland, [http://www.oxycoupage.com/FichiersPDF/Ruukki\\_Pdf/English/Ruukki-Technical-article-Mechanical-and-technological-properties-of-ultra-high-strength-Optim-steels.pdf](http://www.oxycoupage.com/FichiersPDF/Ruukki_Pdf/English/Ruukki-Technical-article-Mechanical-and-technological-properties-of-ultra-high-strength-Optim-steels.pdf)

- [10]. P. Nevasmaa, P. Karjalainen-Roikonen, A. Laukkanen, T. Nykänen, A. Ameri, T. Björk, T. Linnell, J. Kuop, Fracture characteristics of new ultra-high-strength steel with yield strengths 900 – 960 MPa, [http://www.oxycoupage.com/FichiersPDF/Ruukki\\_Pdf/English/Ruukki-Technical-article-Fracture-characteristics-of-new-ultra-high-strength-steel.pdf](http://www.oxycoupage.com/FichiersPDF/Ruukki_Pdf/English/Ruukki-Technical-article-Fracture-characteristics-of-new-ultra-high-strength-steel.pdf)
- [11]. Paul Kaha, Markku Pirinen, Ramio Suoranta, Jukka Martikainen, Welding of Ultra High Strength Steels, Advanced Materials Research Vol. 849 (2014) pp 357-365
- [12] P. Leiviskä , A. Fellman , R. Laitinen , and M. Vänskä , “ Strength properties of laser and laser hybrid welds of low alloyed high strength steels,” in Proceedings of Nolamp Conference, Lappeenranta, Finland (2007).
- [13] A. Fellman, “ Welding of Optim 960 QC steel,” Internal Report No. RR038 of Ruukki (2008).
- [14]. Björk T., Toivonen J., Nykänen T., Capacity of fillet welded joints made of ultra high strength steel, Laboratory of Fatigue and Strength, Lappeenranta University of Technology
- [15]. Ilkka Valkonen, Fracture Toughness of Welded Joints made of UHSS Steel with a Yield Strength of 960 MPa, Proceedings of the Twenty-fifth (2015) International Ocean and Polar Engineering Conference, Kona, Big Island, Hawaii, USA, June 21-26, 2015
- [16]. Wei Guo, Laser Welding of High Strength Steels, Doctoral Thesis, University of Manchester, December 2015